Nuclear Materials and Energy 38 (2024) 101568

Contents lists available at ScienceDirect

Nuclear Materials and Energy

journal homepage: www.elsevier.com/locate/nme

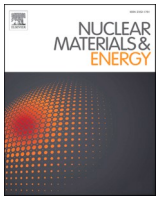

Simulation and study of the milling parameters on CuFeTaTiW multicomponent alloy

R. Martins [a], A.P.Gonçalves [b], J.B. Correia [c], A.Galatanu [d], E. Alves [a], M. Dias [a,*]

[a] Instituto de Plasmas e Fusão Nuclear, Instituto Superior Técnico, Universidade de Lisboa, Av. Rovisco Pais, 1049-001 Lisboa, Portugal
[b] C2TN, DECN, Instituto Superior Técnico, Universidade de Lisboa, Campus Tecnológico e Nuclear, Estrada Nacional 10, 2695-066 Bobadela LRS, Portugal
[c] LNEG, Laboratório Nacional de Energia e Geologia, Estrada do Paço do Lumiar, 1649-038 Lisboa, Portugal
[d] National Institute of Materials Physics, Strada Atomistilor 405A, 077125 Ilfov, Magurelle, Romania

ARTICLE INFO

Keywords:
High entropy alloys
Molecular dynamics
Monte Carlo simulation
Microstructure, mechanical alloying parameters

ABSTRACT

The CuFeTaTiW multicomponent alloy has been devised as an interlayer thermal barrier in nuclear fusion reactors. In order to predict the phase constitution of this alloy, two different lines of work were performed: (a) simulation using Molecular dynamics and Monte Carlo and (b) study of the influence of mechanical alloying parameters on the structures formed. The simulation results show that the most stable structure is achieved starting from a bcc type-structure and using Monte Carlo simulation. In fact, in these conditions the separation into two bcc phases Fe-Ta-W and Cu-Ti is predicted at room temperature. However, the experimental preparation of the materials with mechanical alloying revealed that from 2 h of milling a single bcc phase is formed. The structure of the milled powder was not much influenced by the amount of the process control agent and the by the size of the W starting particles, but generally there was formation of Ta_2H from the reaction between the powders and the process control agent.

1. Introduction

The increase in energy consumption together with the necessity to have clean energy sources leads to nuclear energy being vital. Nuclear fusion reactors can convert the energy released by controlled nuclear fusion into thermal energy for further conversion to mechanical or electrical forms, with no emission of harmful greenhouse gases and no long-lived radioactive waste. To achieve optimal conditions in a nuclear reactor it is essential to have materials capable to withstand the fusion reactor environment. One important part of the tokamak is the divertor, in which the selected materials are tungsten as a plasma-facing component, and CuCrZr alloy as a heat sink [1]. Currently, the main drawback for heat removal is the gap between the operating temperature of the plasma-facing component (W should operate at 623–673 K) due to the ductile–brittle transition behavior (DBTT) [2] and the CuCrZr cooling tubes (service temperature should be between 453 K −573 K) [3]. Therefore, an interlayer between these two materials is needed for efficient heat exchange and extended service lifetimes.

It was suggested by Yeh [4] that $CuCoNiCrAl_xFe$ systems, under certain conditions, can form a solid solution of mixing equal (equiatomic) or relatively large proportions (non-equiatomic) of five or more elements with higher mixing entropies, and therefore favor the formation of multi-element solid solution phases. Therefore these materials called high entropy alloys (HEAs) can have desirable properties for the present application such as high hardness [5] and, oxidation [6] corrosion [7], and irradiation resistance [8], as well as high thermal stability [9]. Owing to the mass and size differences between some of the elements of the proposed compositions, strong phonon and electron scattering will result in low thermal conductivities [10], as required for the interlayer. To date, a large number of HEAs systems have been investigated, which typically include Fe, Al, Cu, Ti, Mg, and Ni [11]. The use of refractory-element-based HEAs (Mo, Nb, Ta, W, and V) was introduced by Senkov et al. [12] mainly as candidates for structural applications at temperatures above 1375 K. Moreover, studies on $W_{0.5}(TaTiVCr)_{0.5}$ high entropy alloy shows a better irradiation resistance when compared with pure W [13]. The numerous systems combinations and the production processes available to prepare these materials render the knowledge of their properties limited. Also, the development of this kind of materials for nuclear fusion reactors applications impose restrictions on the choice of the elements. In particular, low activation elements should be applied for environmental and safety considerations, as well as the transmutation of the alloying elements due

* Corresponding author.
E-mail address: marta.dias@ctn.tecnico.ulisboa.pt (M. Dias).

https://doi.org/10.1016/j.nme.2023.101568
Received 9 October 2023; Received in revised form 15 December 2023; Accepted 20 December 2023
Available online 30 December 2023

to heavy irradiation with highly energetic fusion neutrons. The, Cu, Fe and Ti are considered elements that accomplish the criterium of low level of radioactive waste but the activity values depend on the amount of the element present in the particular component and its location [1415].

In this work is proposed the study of a interlayer with Cu and W, to be used on the divertor section of the nuclear fusion reactor. Moreover, the use of CuFeTaTiW multicomponent alloy is expected to reduce the mismatch between W and the CuCrZr in particular the temperature difference. However, to measure and understand the thermal properties of the samples, the role of each element in the final composition as well and the phases formed is needed.

Therefore, the present work shows the study of the i) simulation of the phases formed on the equiatomic CuFeTaTiW multicomponent alloy together with the ii) production of the equiatomic CuFeTaTiW multicomponent alloy and a complete investigation on the methods of production evolving mechanical alloying and sintering. Moreover, the powder morphology and evolution with milling as well as the phases formed during the milling process are discussed.

2. Materials and methods

An equiatomic CuFeTaTiW multicomponent alloy was simulated using periodic boundary conditions. The software LAMMPS of Sandia Labs [16] was used for a) Molecular Dynamics (MD), b) hybrid Molecular Dynamic/Monte Carlo simulations (MC) and c) X-ray diffraction calculation of MD and MC simulated materials. For bcc simulations the number of atoms was 4394 (13^3 cells) and for fcc simulations the number of atoms was 4000 (10^3 cells). The typical sequence of simulation involved several steps of energy minimization of the initial configuration, heating to the simulation temperature and energy minimization for a period of $6x10^6$ time steps. The hybrid Molecular Dynamic /Monte Carlo simulation, hereafter referred as MC, consisted in the introduction of a Monte Carlo swap attempt every 10 Molecular Dynamic simulation steps. Atomic-swap operations (MC attempts) were performed on randomly-chosen pairs of different types atoms. The temperature used in the Metropolis criterion dictating swap probabilities was the same as that of the isothermal MD simulation. A similar approach was recently used for simulation of a HEA [17]. Pressure was maintained at 1 atmosphere, the simulation used an isothermal–isobaric ensemble (NPT) in LAMMPS. The embedded atom method (EAM) potential for CuFeTaTiW was retrieved from NIST [18] referring to the original work of Zhou et al [19]. The same procedure, using the same data set for simulation of a binary alloy, has been reported in the literature [20]. A wavelength of 1.541838 Ã… for K alpha weighted-mean, was used in the X-ray diffraction simulation. This simulation used the procedures described in [21] and [22].

Powders of Cu, Fe, Ti, Ta (AlfaAesar, 99.9 % nominal purity with average particle size 10 μm) and W (AlfaAesar, 99.9 % nominal purity with average particle size 10 μm and 35–55 nm) were mixed on an equiatomic proportion in a glove box and mechanically alloyed using a high-energy planetary ball mill, PM 400 MA, with WC balls and vials. The balls to powder mass ratio was 10:1, and the milling was performed at different rpm (rotations per minute) and times for milling. The milling conditions were changed and ethanol was used as process control agent (PCA). The sample and the respective atomic percentages are showed in Table 1.

The samples were consolidated by spark plasma sintering (SPS) processing in an FCT Systeme Gmbh sintering machine using a graphite molds. The samples were then sealed under vacuum ($5x10^{-3}$ Pa), using a temperature of 1160 °C with pressures of 76 MPa with a holding time of 5 min then cooled to room temperature. The final discs produced have a volume of 0.53 cm^3 with an average weight of 4.5 g.

Table 1
Atomic percentage of each element in the sample.

Designation	Cu (at.%)	Fe (at.%)	Ta (at.%)	Ti (at.%)	W (at.%)
CuFeTaTiW	20	20	20	20	20

Powder X-ray diffraction (PXRD) was used to investigate the evolution of the powders' mixtures using a Philips X'Pert diffractometer in a Bragg-Brentano geometry with Cu Kα radiation, over a 2θ range from 10° to 100° with a 2 θ step size of 0.03°. The microstructures were observed in backscattered electron imaging (BSE) and secondary electron imaging (SE) modes using a JEOL JSM-7001F field emission gun scanning electron microscope (SEM) equipped with an Oxford Instruments X-ray EDS system.

Thermodynamics calculations were first performed to determine the possible structures formed in the alloys, and to help with the interpretation and discussion of the results. Based on the enthalpies and entropies of mixing, ΔH_{mix} and ΔS_{mix}, the fractional atomic size differences δ and the valence electron concentrations, VEC, it is possible to predict the formation of solid solutions [2324]. Each one can be calculated by the follow equation:

$$\Delta H_{mix} = \sum_{i=1, i\neq j}^{n} \Omega_{ij} c_i c_j \quad (1)$$

where $\Omega_{ij} = 4\Delta_{mix}^{AB}$ and Δ_{mix}^{AB} is the mixing enthalpy of binary liquid AB alloys, and c_i and c_j are the concentration of the elements,

$$\Delta S_{mix} = R\sum_{i=1}^{n} c_i ln c_i \quad (2)$$

where R is the gas constant,

$$\delta = 100\sqrt{\sum_{i=1}^{n} c_i(1 - r_i/\bar{r})^2} \quad (3)$$

where c_i and r_i are the atomic radius of the ith element and r is given by:

$$\bar{r} = \sum_{i=1}^{n} c_i r_i \quad (4)$$

$$VEC = \sum_{i=1}^{n} c_i (VEC)_i \quad (5)$$

where $(VEC)_i$ is the valence electron concentration for each ith element.

A solid solution can be formed in the ranges -15 kJ/mol $\leq \Delta H_{mix} \leq$ 5 kJ/mol, 11 J/(K·mol) $\leq \Delta S_{mix} \leq$ 19.5 J/(K·mol), and $1 \leq \delta \leq 6$. The most stable phases predicted were the fcc for VEC ≥ 8 and bcc for VEC $<$ 6.87. Between these values, mixed fcc and bcc type-structures are expected to coexist. In this context, calculations of the relevant properties of CuFeTaTiW multicomponent alloy are presented in Table 2. Based on the calculated values, and since δ is higher than 6, the existence of a solid solution is not expected for the equiatomic composition.

3. Results

3.1. Simulation

Fig. 1 shows the results for (a) molecular dynamics (MD) and (b) Monte Carlo (MC) simulations for the CuFeTiTaW multicomponent high entropy alloy at 300 K, starting with a bcc and a fcc type-structure.

The simulations were started randomly distributing the constituent chemical elements throughout the lattice sites (either bcc or fcc). When a purely MD simulation was performed there was no evidence of chemical

Table 2
Thermodynamic calculations for CuFeTaTiW multicomponent alloy.

Results	
ΔH_{mix}	−2,56 kJ/mol
ΔS_{mix}	13.38 J/(K mol)
Δ	6.25
VEC	6.8

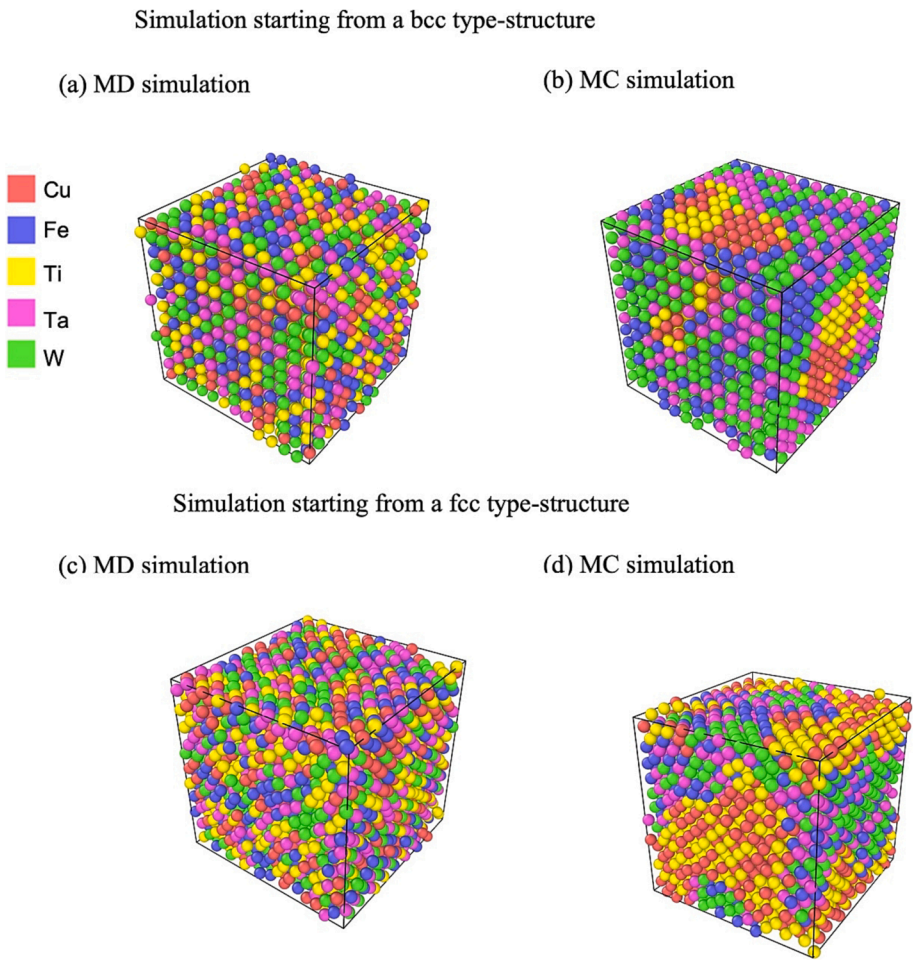

Fig. 1. Representation of the structures simulated starting from bcc type-structure at 300 K with (a) Molecular dynamics and (b) Monte-Carlo and the structures simulated starting from fcc type-structure at 300 K with (c) Molecular dynamics and (d) Monte-Carlo.

segregation suggesting the formation of a HEA as shown in Fig. 1 (a) and (c). When a MC simulation was used, either starting from bcc or fcc, chemical segregation was evident, resulting in phase separation (Fe-Ta-W) and (Cu-Ti). In what pertains to the crystal structure, the simulations starting from bcc, both MD and MC, yielded a final configuration exclusively of bcc type structures. For the simulations started with fcc type-structure, in both MD and MC simulation, the final result was a combination of two phases one bcc (Fe-Ta-W) and a fcc type-structure (Cu-Ti). Fig. 2 shows the potential energy versus temperature for the various starting structures and simulation procedures. The lowest potential energy in this HEA system was obtained when starting from a bcc type-structure with the five elements randomly distributed over lattice positions and using MC simulation, as can be observed in blue dots in Fig. 2. The most stable structure, corresponding to the lowest potential

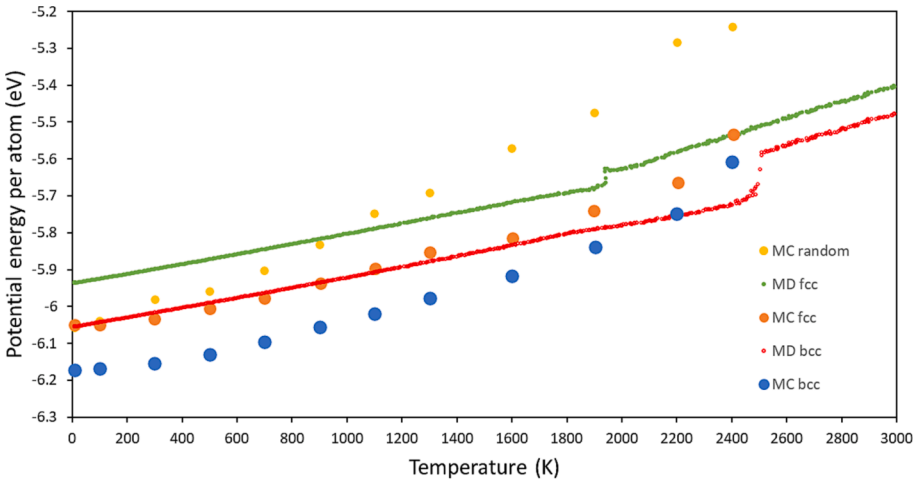

Fig. 2. Potential energy versus temperature calculated via MD and MC starting from a bcc and a fcc type-structures.

energy (Ep) configuration is achieved with phase separation of chemical species (Fe-Ta-W) and (Cu-Ti) whilst maintaining the overall bcc crystal structure (Fig. 1 (b)).

However, close to the melting point in MD simulation (see red dots in Fig. 2) provide the lowest potential energy. This indicates that the un-segregated structure, e.g Fig. 1 (a) is more stable at high temperatures. The results of a more detailed calculation, the free energy variation considering the configuration entropy, i.e. the ΔG of the reaction:

$$(Cu,Fe,Ta,Ti,W)_{bcc} \rightarrow (Fe,TaW)_{bcc}+(Cu,Ti)_{bcc} \quad (1)$$

is presented in Fig. 3.

These results indicate that a segregated bcc type-structure with two phases (Fe-Ta-W) and (Cu-Ti) would be stable up to ~ 1500 K, whereas above that temperature and up to melting (~2500 K) a true HEA without segregation would be the stable phase.

Simulations starting from non-random lattice positions, i.e amorphous structure, shown in Fig. 4 (a) resulted in absence of crystallization and much higher potential energy values, (Fig. 2) than those of simulations starting from lattice positions. However, for very low temperature, below 100 K, potential energy is comparable to that of the MD simulation starting from bcc type-structure (Fig. 2). This relative stability of the amorphous phase at low temperature is achieved through phase separation (segregation) similar to that of the MC simulations starting from lattice positions. The simulations evidence a strong tendency for phase separation in this system, even in amorphous structures.

The simulated XRD patterns of MC simulation at 300 K starting from bcc are shown in Fig. 5. These patterns were obtained separately with LAMMPS from the two bcc completely segregated phases, as can be seen in Fig. 1 (b). The corresponding lattice parameters fitted to the two phases are virtually identical, respectively 0.3101 nm (Fe-Ta-W) and 0.3101 nm (Cu-Ti). This is visible in the shoulder at about 30° in Fig. 5 (see the red arrow), corresponding to an extra reflection of a B2 type-structure are associated with the Fe–Ta–W phase.

The simulated XRD pattern of a single-phase MD simulation at 300 K starting from a bcc type-structure, is shown in Fig. 6 (a) and the global XRD simulation of MC at 300 K is shown Fig. 6 (b).

Again, bcc structures with lattice parameters of respectively 0.3114 nm (MD simulation) and 0.3108 nm (MC simulation) are indexed. It can thus be concluded that a small lattice parameter contraction (-0.2 %) is induced via phase separation, (-0.4 %) considering the XRD fittings obtained separately from the MC simulated phases.

The radial distribution function g(r) obtained from Fe-Ta-W phase in MC simulation at 300 K starting from bcc type-structure is shown in Fig. 7. The same can be inferred from Fig. 7, where in the g(r) for Fe-Fe the signal of the 1NN is virtually inexistent, clearly indicating ordering within the bcc type-structure. It evidences the distance of the first four nearest neighbors (NN) typical of a bcc structure. A significant feature is the low probability of Fe-Fe as first NN, clearly confirming a degree or ordering i.e. a trend towards B2 type intermetallic structure. The radial distribution function g(r) obtained from Cu-Ti phase in MC simulation at 300 K starting from bcc is shown Fig. 8, again it evidences a strong tendency to ordering as the Cu-Ti bond has the highest probability as 1st NN.

The radial distribution function g(r) obtained from CuFeTaTiW alloy in MD simulation at 300 K starting from bcc, is shown in Fig. 9 which evidences a very large dispersion of bond lengths as 1st NN depending on the chemical elements involved: bonds including only Cu and Fe are the shortest ~ 0.255 nm, those including only W and Ta are the longest ~ 0.275 nm. The result of the single phase MD simulation at 300 K is thus a highly distorted structure. It can be speculated that albeit the difference in free energy between the segregated structure and the single solid solution is only 0.1 eV/atom at 300 K (Fig. 3). This is an extremely small driving force for the segregation reaction. In real practical terms phase separation depends on diffusion (slow in HEA) and nucleation, constituting barriers to phase separation. With such small driving force phase separation may not be occur at all. The MC simulation process is not constrained by mechanisms of phase transformation such as diffusion and thus can converge to configurations carrying an extremely small energy gain. On the other hand, the reduction in lattice parameter from MD to MC simulation, producing a more compact structure, and the reduction in lattice distortion would favor such phase separation at low temperatures. In real practical terms, phase separation depends on diffusion (slow in HEA) and on nucleation, which are constituting diffusion barriers.

3.2. Experimental results

3.2.1. Effect of the milling time

Fig. 10 shows the diffractogram of the CuFeTiTaW multicomponent alloy after milling with 20 ml of ethanol at 350 rpm during (a) 0 h, (b) 2 h, (c) 6 h and (d) 12 h. The initial powder mixture (Fig. 10 (a)) presents the peaks of the individual elements Cu, Fe, Ta, Ti and W. The diffractogram for the material milled for 2 h evidenced also the presence of each element with broader peaks, which indicates that the milling time was not enough to promote the alloy formation. After 6 h of milling, due to the collision, cold welding of the particles and to the diffusion of the

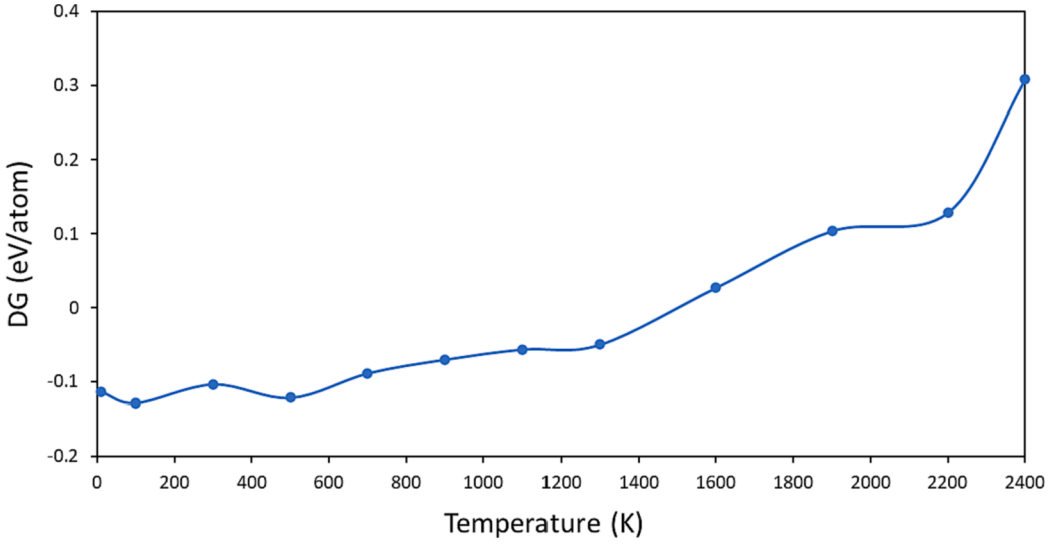

Fig. 3. Free energy variation of bcc separation into two phases.

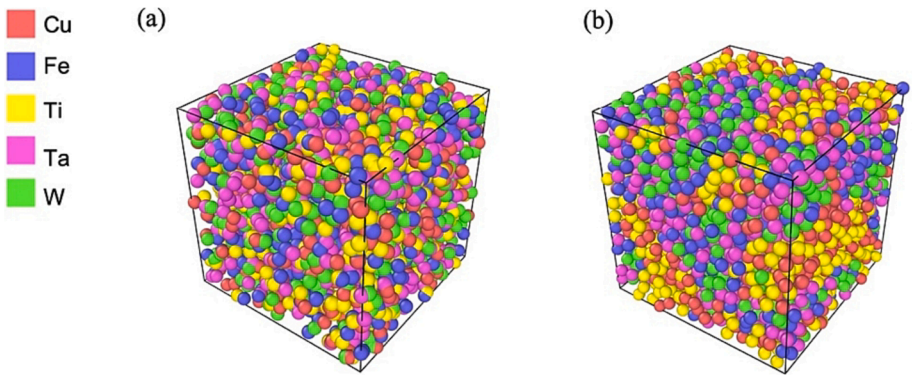

Fig. 4. MC Simulation starting from non-lattice (random) positions at 300 K. (a) starting random amorphous configuration (b) final segregated amorphous configuration.

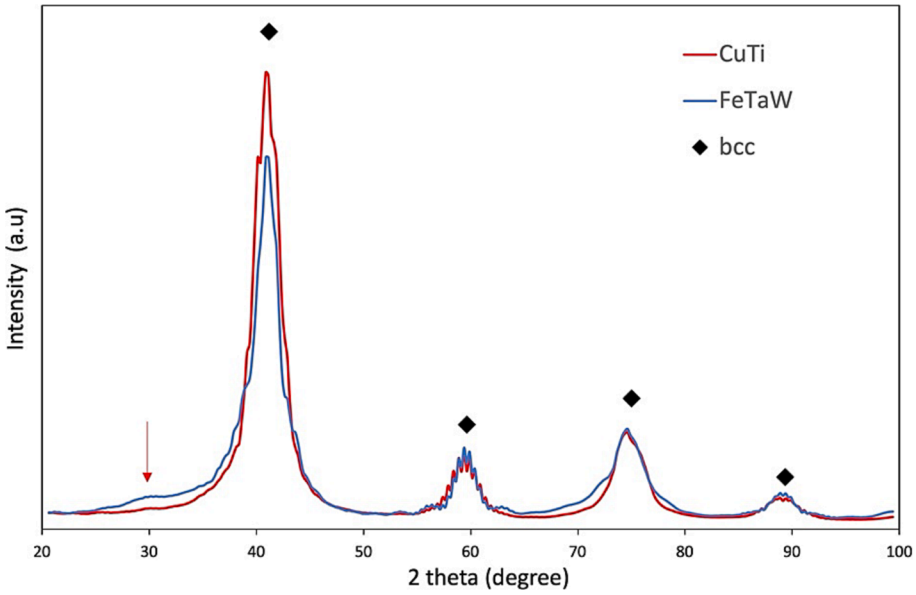

Fig. 5. Simulated XRD patterns of MC simulation at 300 K starting from a bcc structure.

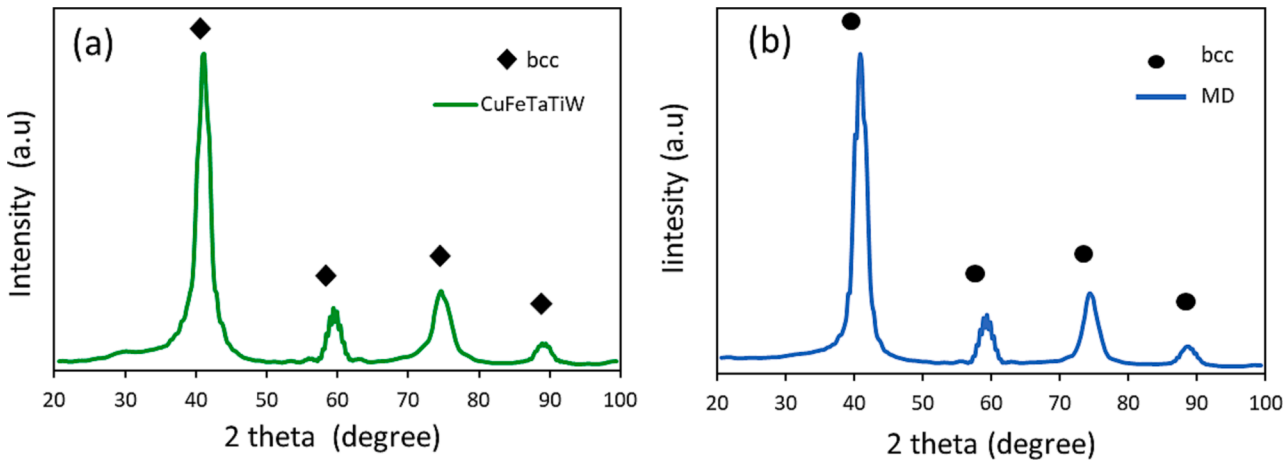

Fig. 6. Simulated XRD patterns of (a) MD and b) MC simulation at 300 K starting from bcc type-structure.

elements into each other's lattice, the peaks of the individual elements decreased and the presence of a bcc type-structure was also identified. Moreover, after 12 h of milling, a bcc type-structure together with the formation of Ta_2H was observed with more intense WC peaks. The reduction and the broadening of the peaks is attributed to the reduction in crystallite size and increase in lattice strain. The lattice parameter for bcc type-structure after 12 h of milling was found to be 0.316 nm close to that of pure W, 0.316 nm [20]. The diffractogram of bcc phase has strong

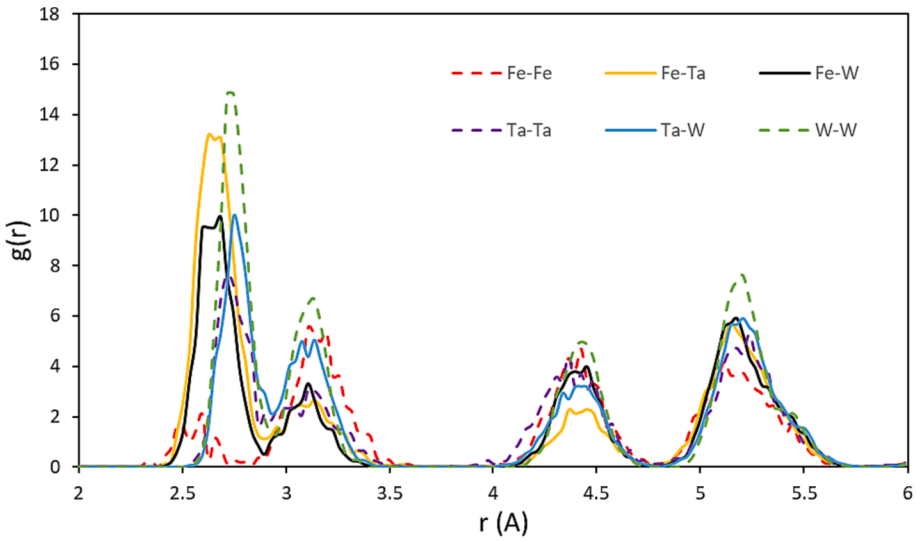

Fig. 7. Radial distribution function g(r) obtained from Fe-Ta-W phase in MC simulation at 300 K.

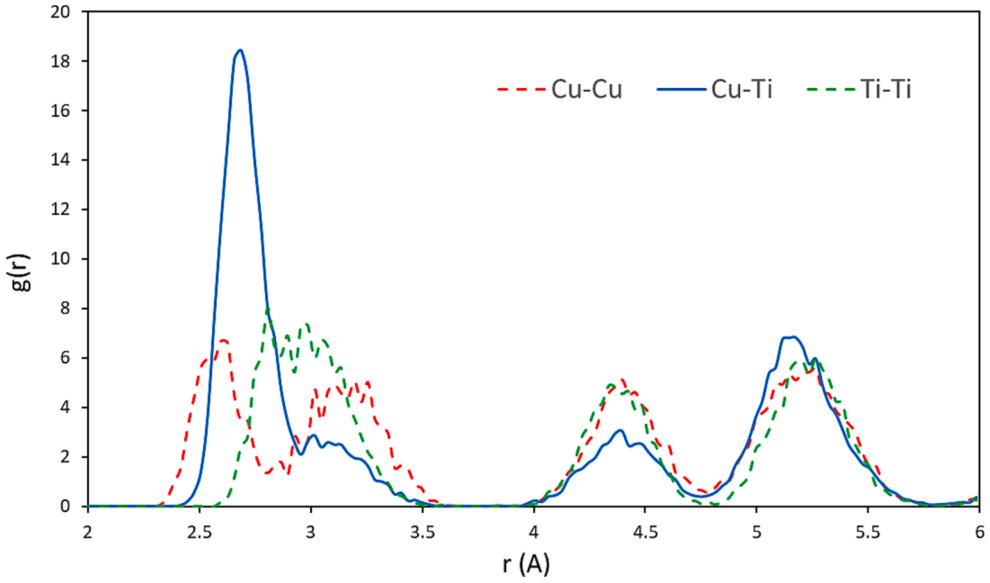

Fig. 8. Radial distribution function g(r) obtained from Cu-Ti phase in MC simulation at 300 K.

scattering signal from W but a large proportion of Ta was lost due to hydride formation. The presence of high melting point metals, as W, hinder the process of metal blending when melting is involved, i.e., they tend to be excluded from the overall multicomponent alloy via mechanisms related to the high melting point. For instance, W has fast work hardening and does not recover below 873 K [25], unlike most transition metals. It therefore remains in the form of hard inclusions [26]. Another issue is the activation energy for diffusion which also correlates with the melting temperature of the metal [27]. After 12 h of milling the peaks of Cu and Fe are faintly visible which allow us to conclude that the mixture of Cu and Fe has progressed.

3.2.2. *Effect of process control agent amount*

Fig. 11 shows the diffractograms of the evolution of the equiatomic CuFeTaTiW multicomponent alloy in two different stages of synthesis: using 20 ml and 4 ml of ethanol as process agent control milled at 350 rpm. The idea of the reduction of the process control agent (PCA) was to avoid the formation of hydrides in the powder as observed in Fig. 10 (d). In fact, the two diffractograms are very similar presenting a bcc type-structure, WC and Ta_2H. The surface of the powder particles milled with 4 ml and 20 ml of ethanol is shown in Fig. 12. The powder has similar morphology in both cases and no contamination was found by EDS in both cases. Moreover, the images revealed that the elements are homogeneous distributed inside the particles.

3.2.3. *Effect of initial W particle size*

In the previous section it was observed that it is very difficult to obtain an homogeneous bcc phase with all the elements. It was thought that the fast work hardening characteristics of W may prevent it to enter the HEA during mechanical alloying (MA) process. In this section it will be discussed the influence of W size particles on the phase formation of the high entropy alloy. An additional attempt of MA was performed using nano and micro powders of W. The X-ray pattern after the milling (4 h) for both type of samples, micron sized W and nano sized W powders is shown in Fig. 13. The formation of Ta_2H was observed after 4 h of milling when the W nano powder was used. Moreover, a bcc type-structure was observed in both cases as was expected with a similar lattice parameter (for W nano powder a = 0.3165 nm and for the W

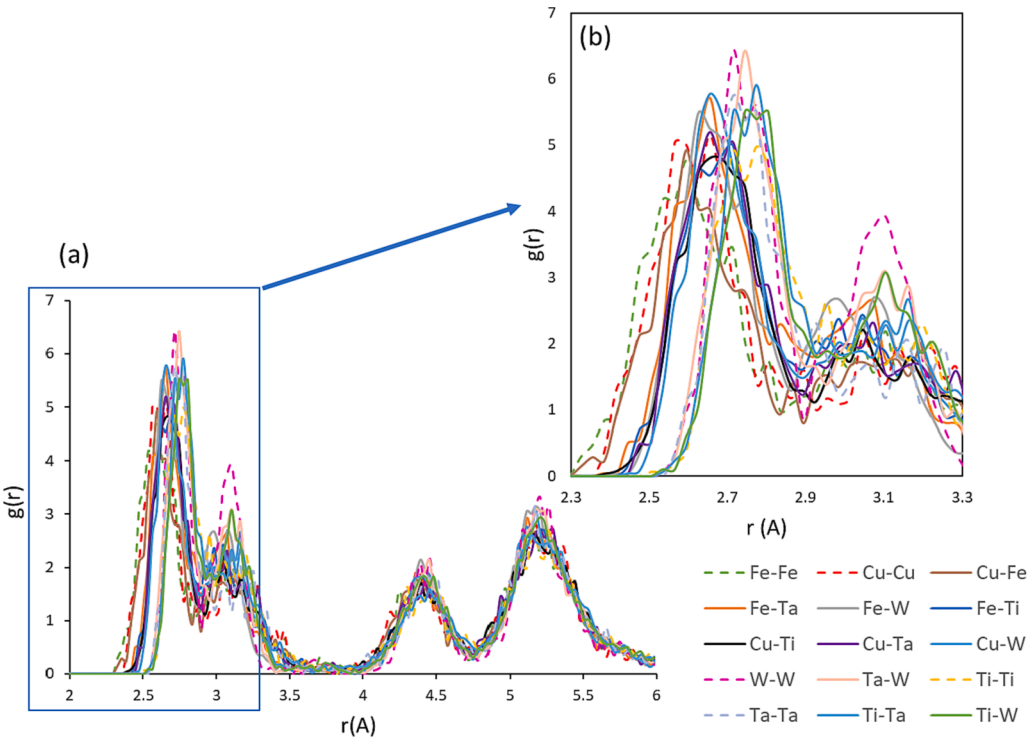

Fig. 9. (a) Radial distribution function g(r) obtained from CuFeTaTiWmulticomponent alloy in MD simulation at 300 K and (b) magnification of selected area.

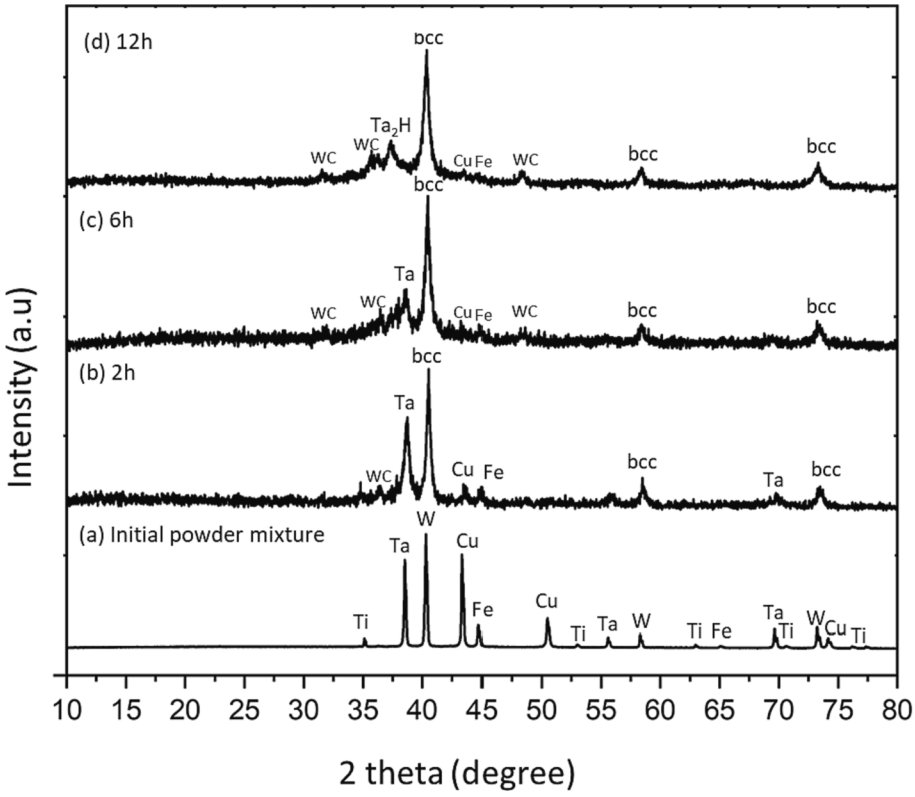

Fig. 10. Experimental diffractogram of the CuFeTaTiW multicomponent milled with 20 ml de ethanol for (a) mixture of the initial powder without milling (b) 2 h, (c) 6 h and (d) 12 h.

micro powder a = 0.3161 nm). The reduction of the grain size of W could have improved the homogeneity of the high entropy alloy, as no major "shoulders" are seen in the diffractogram near the major bcc peak with W nano powder. Nevertheless, the presence of Ta_2H hindered the goal of obtaining a solid solution.

Examining the experimental diffractograms in Fig. 13, it becomes

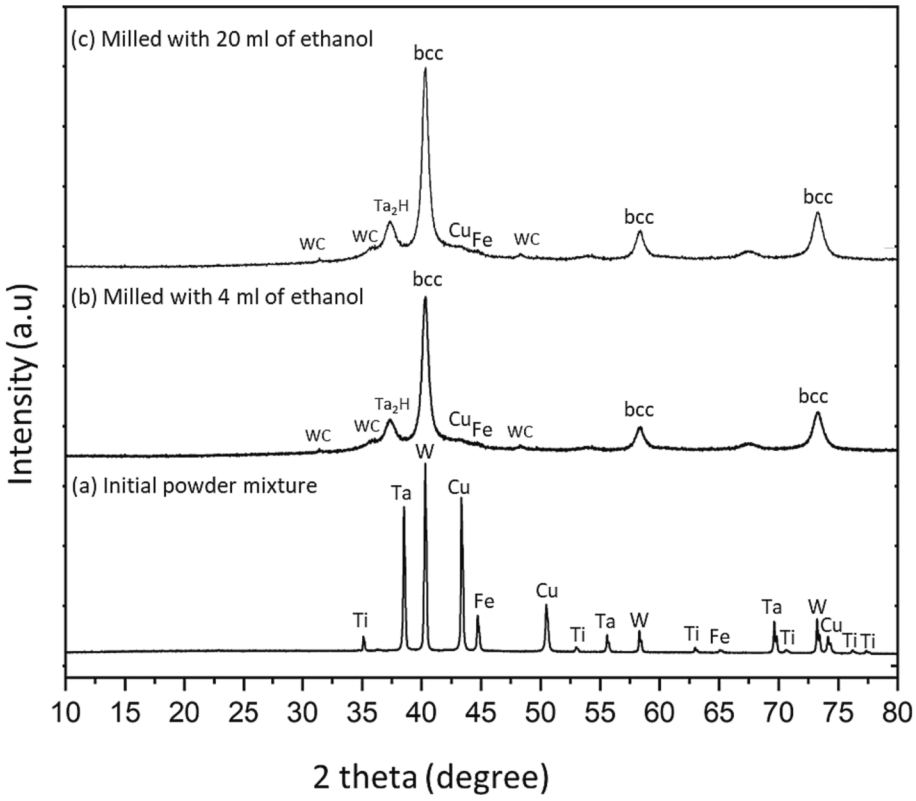

Fig. 11. Experimental diffractogram of the CuFeTaTiW multicomponent of milled with (a) mixture of the initial powder without milling, (b) 4 ml de ethanol and (c) 20 ml de ethanol.

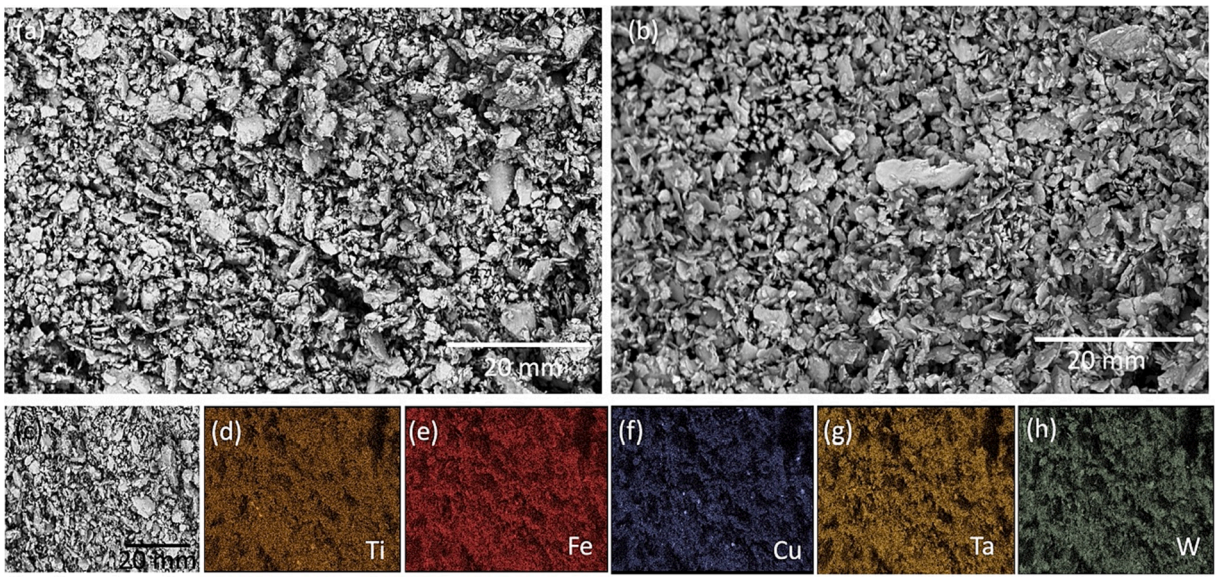

Fig. 12. SEM images of the samples milled with (a) 4 ml of ethanol and (b) 20 ml de ethanol, (c) image of the sample milled with 4 ml of ethanol and EDS map for (d) Ti-Kα, (e) Fe-Kα, (f) Cu-Kα, (g) Ta- Lα and (h) W- Lα lines.

apparent that the lattice parameter of both the micro and nano powder samples is remarkably similar to that of pure tungsten. This similarity is expected due to the dominant yield of the heavier W in the XRD but needs independent confirmation of the presence of pure tungsten in the powder. To ascertain the particle size and identify any pure tungsten particles, scanning electron microscopy (SEM) and energy-dispersive X-ray spectroscopy (EDS) mapping were conducted on the micro and nano powder shown in Fig. 14. A comparison between the micro and nano powder samples reveals that the nano powder sample exhibits smaller particles that tend to cluster around larger particles, a feature not observed in the micro powder alloy, Fig. 14 (a) and (b) respectively. Furthermore, EDS analysis of both the nano and micro powder samples demonstrates the homogeneous dispersion of all elements, with no evidence of pure tungsten particles as showed for the micro powder in Fig. 14 (c) to (h). Table 3 shows the elemental atomic concentration on the powder showed on Fig. 14. Since the initial elemental concentration

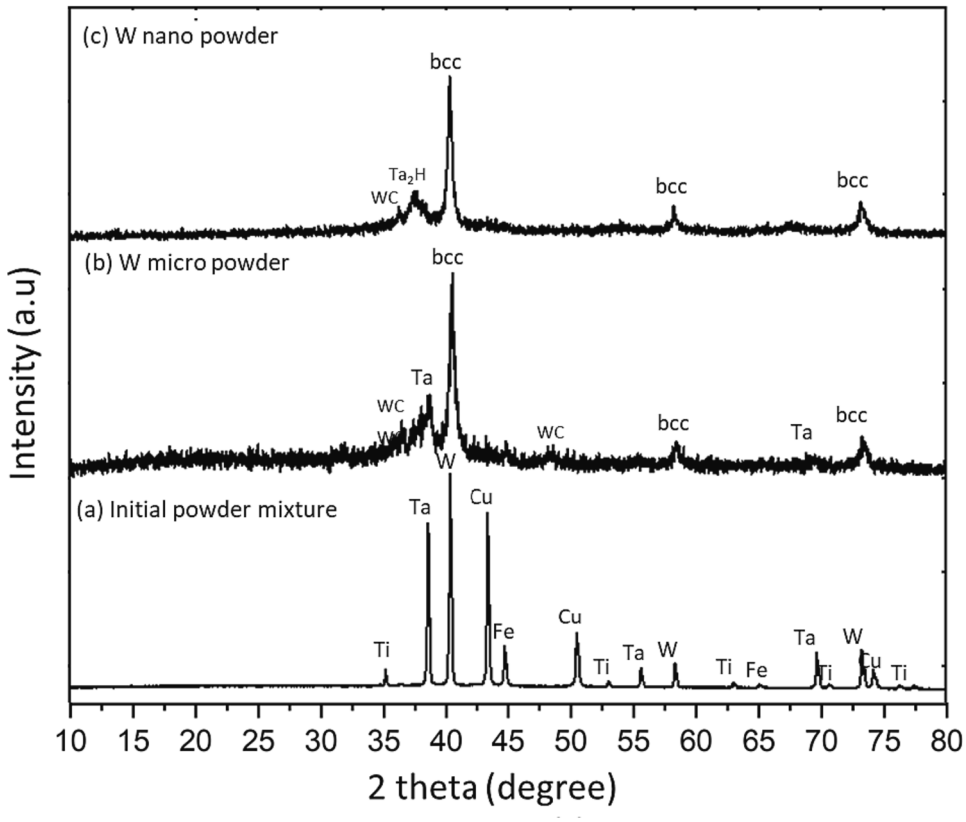

Fig. 13. Experimental diffractogram of the CuFeTaTiW multicomponent of milled with 4 ml of ethanol with (a) mixture of the initial powder without milling, (b) W as a micro powder, and (c) W as a nano powder.

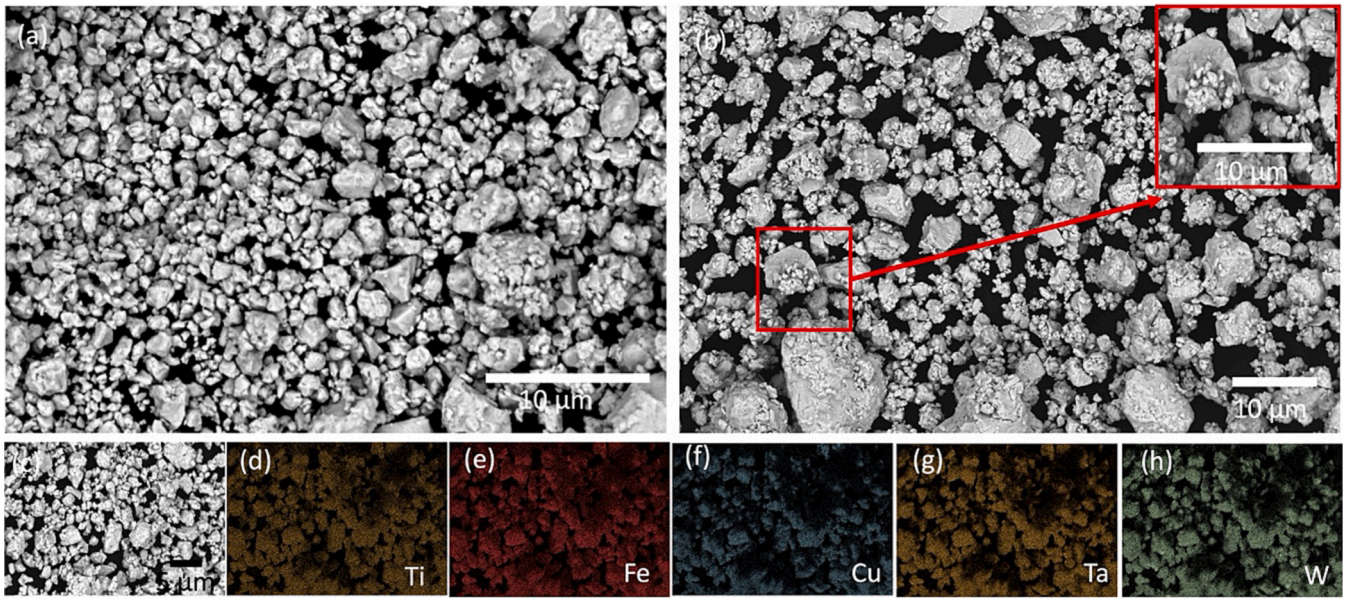

Fig. 14. SEM images of the samples milled with (a) W micro powder, (b)W nano powder, EDS map of the CuFeTaTiW multicomponent of milled with micro-Tungsten (W) powder for (a) SE image, (b) Ti-Kα, (c) Fe-Kα, (d) Cu-Kα, (e) Ta- Lα and (f) W- Lα lines.

was 20 at.%, the values shown in Table 3 are not too much deviated, however with less Ti and Ta.

3.2.4. *Consolidated samples*

This section presents the results of the samples consolidated by SPS process from the powders milled with 4 wt% of ethanol and using W micron particles. SEM images from the consolidated sample are shown Fig. 15. The microstructures obtained by consolidation present a major phase and the presence of bight particles. Moreover, is possible to observe some porosity in the sample surface, which is confirmed by Archimedes methods indicating a densification around 75 %.

EDS maps are shown in Fig. 16 for the SPS consolidated sample. The elemental map shows the existence of an iron and copper rich phases in the samples, while all other elements were dispersed equally throughout

Table 3
EDS map results on the atomic concentration on each element present on the milled powder.

EDS map sesults	
Element	**Atomic concentration %**
Ti	16.842
Fe	22.323
Cu	22.754
Ta	15.922
W	22.159

the surface. Moreover, the bright particles seems to be associated with the enrichment of W.

3.2. Discussion

The results show that increasing the milling time an increase of WC contamination occurs, and the lattice parameters of the bcc formed is similar to the pure W. On the other hand, the microstructure did not revealed the presence of pure W, but evidences the mixture of the elements. These results indicate that probably W is mixed in a high entropy alloy, but this alloy has a similar lattice parameter with pure W. A recent review of the microstructure of W-based high entropy alloys (WNbMoTa and WNbMoTaV [1228]) showed that a single bcc phase was formed, which seems to be in agreement with the present experimental results.

Another relevant aspect is the existence of the solvent on mechanical alloying. In fact, wet milling tends to be a less efficient process than dry milling. However, the milling with elements like Cu, which are ductile is very difficult without a PCA due to the fact that after a few hours the milled powder is glued to the balls and containers. Wet milling is more complex, thanks to the addition of a liquid, but this process also has the power to reduce a product into finer particles. This allows the production of a greater variety of species and avoid the formation of a solid solution high entropy alloy with the initial composition.

However, increasing the PCA amount, a decrease in interdiffusion between particles occurs, due to the formation of the PCA layer on their surface, which increases the distances between the particles. In addition, the process control agent (solvent) can react with some metals and form stable hydrides, as is the case of Ta_2H [29]. Once formed, the stable hydrides can only decompose under specific conditions. In fact, even after heat treated the powder with 1173 K for 1 h the materials produced, it was very difficult to remove such hydrides.

The experimental diffractograms show the presence of a major bcc type-structure with a lattice parameter around 0.316 nm, very similar to pure W. On the other hand, the simulations (MD or MC) evidenced a bcc structure with lattice parameters around 0.311 nm, lower that the experimental ones. Moreover, MC predicted phase separation (Fe-Ta-W) and (Cu-Ti) lowering the internal strains and making structure more compact. However, this kind of process needs nucleation and diffusion, which seem not to occur with the experimental procedure used. In fact,

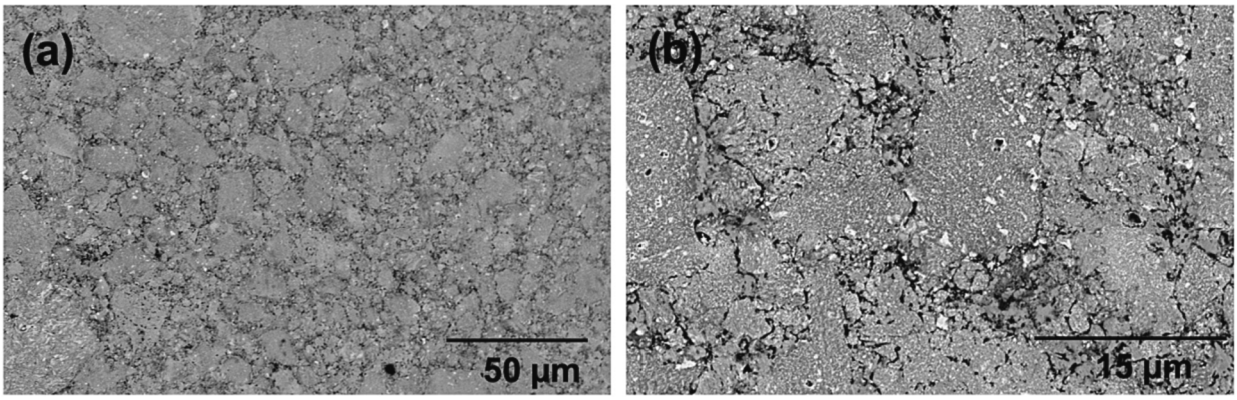

Fig. 15. Microstructure of the CuFeTaTiW consolidated sample with (a) and (b) SPS at 1160 °C.

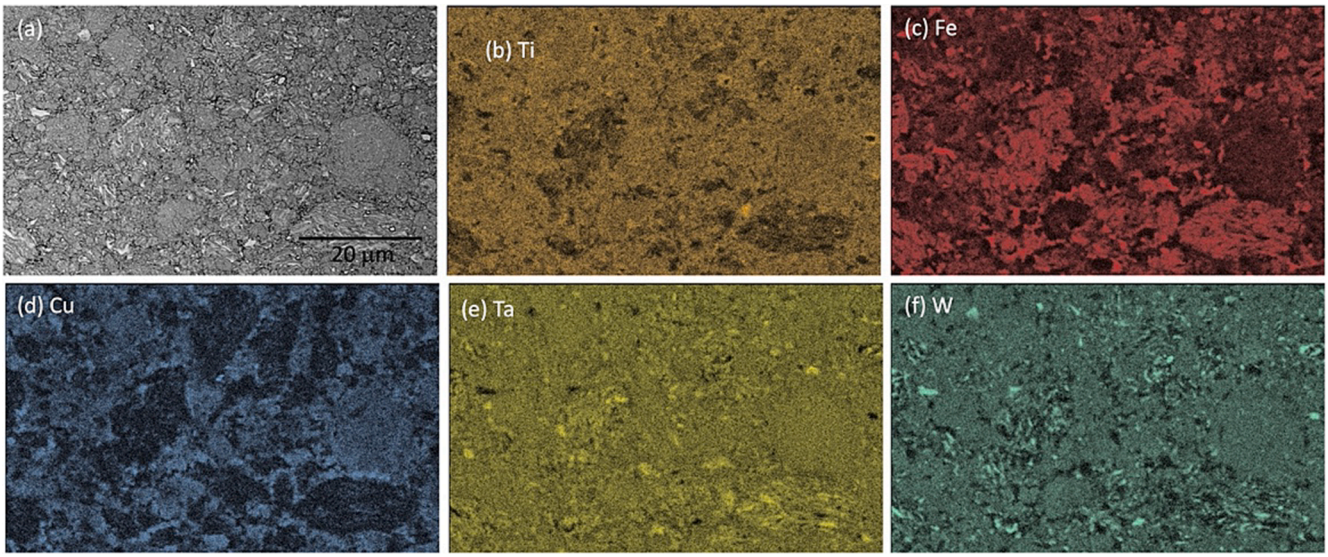

Fig. 16. (a) SE image of the CuFeTaTiW consolidated sample via SPS and EDS elemental maps for (b)Ti- Kα, (c) Fe-Lα, (d) Cu-Lα, (e) Ta- Lα and (f) W-Lα lines.

the milling time can be as long as 40 h [303132], which can effectively promote the nucleation and diffusion of a second phase. In the present case and due to the use of PCA, which favors the hydrides formation together with the aim of reducing contamination with the milling media, the milling time was reduced. In fact the consolidated material evidenced the presence of Ta particles which can result from the Ta not mixed and probably from the hydrides formed.

4. Conclusions

The equiatomic CuFeTaTiW multicomponent alloy to be used as a thermal barrier interlayer in nuclear fusion reactors was prepared by mixing the elements in a glove box and milling. The study of the influence of mechanical alloying parameters on the structures formed was performed. Also, the simulation of the phase constitution and crystal structures formed was performed using Molecular dynamics and Monte Carlo. The simulation results point to the formation of the most stable structure starting from a bcc type-structure and using Monte Carlo method. In addition, using MC at room temperature phase separation into two bcc type-structures Fe-Ta-W and Cu-Ti with a similar lattice parameter, 0.3101 nm, close to that obtained experimentally (0.316 nm). With increasing time of milling the diffractograms evidence after 12 h that the individual peaks of the elements disappear, which points to the formation of a bcc solid solution with a lattice parameter similar to the pure W. Moreover, reducing the amount of PCA seems to promote the W mixture. The particle size of W doesn't influence the Ta_2H formation.

To conclude, the lattice parameter found on the MC simulation starting from a bcc type-structure is relatively close to that found on the experimental diffractograms. The phase constitution predicted with MC simulation, separation into two bcc phases, did not occur with the present experimental procedure conditions, which may be associated with slow diffusion and nucleation in HEAs.

Declaration of competing interest

The authors declare that they have no known competing financial interests or personal relationships that could have appeared to influence the work reported in this paper.

Data availability

Data will be made available on request.

Acknowledgements

This work has been carried out within the framework of the EUROfusion Consortium, funded by the European Union via the Euroatom Research and Training Program (Grant Agreement No 101052200 â EUROfusion). Views and opinions expressed are however those of the author(s) only and do not necessary reflect those of the European Union or the European Commision. Neither the European Union nor the European Comission can be held responsible for them. IPFN activities received financial support from "Fundação para a Ciência e Tecnologia" through projects UIDB/50010/2020, UID/Multi/04349/2019 and PTDC/FIS-PLA/31629/2017.

References

[1] R.A. Pitts, S. Bardin, B. Bazylev, M.A. van den Berg, P. Bunting, S. Carpentier-Chouchana, J.W. Coenen, Y. Corre, R. Dejarnac, F. Escourbiac, J. Gaspar, J. P. Gunn, T. Hirai, S.-H. Hong, J. Horacek, D. Iglesias, M. Komm, K. Krieger, C. Lasnier, G.F. Matthews, T.W. Morgan, S. Panayotis, S. Pestchanyi, A. Podolnik, R.E. Nygren, D.L. Rudakov, G. De Temmerman, P. Vondracek, J.G. Watkins, Physics conclusions in support of ITER W divertor monoblock shaping, Nucl. Mater. Energy 12 (2017) 60–74.
[2] P. Gumbsch, Brittle fracture and the brittle-to-ductile transition of tungsten, J. Nucl. Mater. 323 (2–3) (2003) 304–312.
[3] D. Stork, P. Agostini, J.L. Boutard, D. Buckthorpe, E. Diegele, S.L. Dudarev, C. English, G. Federici, M.R. Gilbert, S. Gonzalez, A. Ibarra, C.h. Linsmeier, A. Li Puma, G. Marbach, P.F. Morris, L.W. Packer, B. Raj, M. Rieth, M.Q. Tran, D. J. Ward, S.J. Zinkle, Developing structural, high-heat flux and plasma facing materials for a near-term DEMO fusion power plant: The EU assessment, J. Nucl. Mater. 455 (1-3) (2014) 277–291.
[4] J.-W. Yeh, S.-K. Chen, S.-J. Lin, J.-Y. Gan, T.-S. Chin, T.-T. Shun, C.-H. Tsau, S.-Y. Chang, Nanostructured high-entropy alloys with multiple principal elements: Novel alloy design concepts and outcomes, Adv. Eng. Mater. 6 (5) (2004) 299–303.
[5] C.-J. Tong, M.-R. Chen, J.-W. Yeh, S.-J. Lin, S.-K. Chen, T.-T. Shun, S.-Y. Chang, Mechanical performance of the AlxCoCrCuFeNi high-entropy alloy system with multiprincipal elements, Metall. Mater. Trans. A 36 (5) (2005) 1263–1271.
[6] P.-K. Huang, J.-W. Yeh, T.-T. Shun, S.-K. Chen, Multi-Principal-Element Alloys with Improved Oxidation and Wear Resistance for Thermal Spray Coating, Adv. Eng. Mater. 6 (12) (Feb. 2004) 74–78.
[7] Y.Y. Chen, U.T. Hong, H.C. Shih, J.W. Yeh, T. Duval, Electrochemical kinetics of the high entropy alloys in aqueous environments - a comparison with type 304 stainless steel, Corros. Sci. 47 (11) (2005) 2679–2699.
[8] O. El-Atwani, N. Li, M. Li, A. Devaraj, J.K.S. Baldwin, M.M. Schneider, D. Sobieraj, J.S. Wróbel, D. Nguyen-Manh, S.A. Maloy, E. Martinez, Outstanding radiation resistance of tungsten-based high-entropy alloys, Sci. Adv. 5 (3) (2019).
[9] M.-H. Tsai, C.-W. Wang, C.-W. Tsai, W.-J. Shen, J.-W. Yeh, J.-Y. Gan, W.-W. Wu, Thermal stability and performance of NbSiTaTiZr high-entropy alloy barrier for copper metallization, J. Electrochem. Soc. 158 (11) (2011) H1161.
[10] H.P. Chou, Y.S. Chang, S.K. Chen, J.W. Yeh, Microstructure, thermophysical and electrical properties in AlxCoCrFeNi ($0 \leq x \leq 2$) high-entropy alloys, Mater. Sci. Eng. B Solid-State Mater. Adv. Technol. 163 (3) (2009) 184–189.
[11] J.-W. Yeh, Recent progress in high-entropy alloys, Eur. J. Control - EUR J Control 31 (6) (2006) 633–648.
[12] O.N. Senkov, G.B. Wilks, D.B. Miracle, C.P. Chuang, P.K. Liaw, Refractory high-entropy alloys, Intermetallics 18 (9) (Sep. 2010) 1758–1765.
[13] O.A. Waseem, H.J. Ryu, Helium ions irradiation analysis of W0.5(TaTiVCr)0.5 for application as a future fusion plasma-facing material, Mater. Chem. Phys., vol. 260, no. December 2020, p. 124198, 2021.
[14] M.R. Gilbert, et al., Waste implications from minor impurities in European DEMO materials, Nucl. Fusion 59 (7) (Jul. 2019) 076015.
[15] D. Stork, et al., Materials R&D for a timely DEMO: Key findings and recommendations of the EU Roadmap Materials Assessment Group, Fusion Eng. Des. 89 (7–8) (Oct. 2014) 1586–1594.
[16] A.P. Thompson, et al., LAMMPS - a flexible simulation tool for particle-based materials modeling at the atomic, meso, and continuum scales, Comput. Phys. Commun. 271 (Feb. 2022) 108171.
[17] S. Chen, et al., Chemical-affinity disparity and exclusivity drive atomic segregation, short-range ordering, and cluster formation in high-entropy alloys, Acta Mater. 206 (Mar. 2021) 116638.
[18] https://www.ctcms.nist.gov/potentials/, "NIST." .
[19] X.W. Zhou, R.A. Johnson, H.N.G. Wadley, Misfit-energy-increasing dislocations in vapor-deposited CoFe/NiFe multilayers, Phys. Rev. B 69 (14) (Apr. 2004) 144113.
[20] J.R. Rumble, T.J. Bruno, M.J. Doa, CRC handbook of chemistry and physics : a ready-reference book of chemical and physical data.
[21] S. Plimpton, Fast Parallel Algorithms for Short-Range Molecular Dynamics, 1995.
[22] S.P. Coleman, D.E. Spearot, L. Capolungo, Virtual diffraction analysis of Ni [0 1 0] symmetric tilt grain boundaries, Model. Simul. Mater. Sci. Eng. 21 (5) (Jul. 2013) 055020.
[23] S. Guo, C.T. Liu, Phase stability in high entropy alloys: Formation of solid-solution phase or amorphous phase, Prog. Nat. Sci. Mater. Int. 21 (6) (2011) 433–446.
[24] Y. Zhang, Y.J. Zhou, J.P. Lin, G.L. Chen, P.K. Liaw, Solid-solution phase formation rules for multi-component alloys, Adv. Eng. Mater. 10 (6) (2008) 534–538.
[25] D. Brunner, Peculiarities of work hardening of high-purity tungsten single crystals below 800 K, vol. 389, pp. 167–170, 2004.
[26] F. Ren, W. Zhu, K. Chu, C. Zhao, Tribological and corrosion behaviors of bulk Cu e W nanocomposites fabricated by mechanical alloying and warm pressing, J. Alloys Compd. 676 (2016) 164–172.
[27] E.R.S.M. Gupta, Devendra, Diffusion Processes in Advanced Technological Materials.
[28] S. Chen, C. Qi, J. Liu, J. Zhang, Y. Wu, Recent advances in W-containing refractory high-entropy alloys—an overview, Entropy 24 (11) (Oct. 2022) 1553.
[29] M.V. Lototskyy, V.A. Yartys, B.G. Pollet, R.C. Bowman, Metal hydride hydrogen compressors: a review, Int. J. Hydrogen Energy 39 (2014) 5818–5851.
[30] C. Wang, W. Ji, Z. Fu, Mechanical alloying and spark plasma sintering of CoCrFeNiMnAl high-entropy alloy, Adv. Powder Technol. 25 (4) (Jul. 2014) 1334–1338.
[31] W. Ji, W. Wang, H. Wang, J. Zhang, Y. Wang, F. Zhang, Z. Fu, Alloying behavior and novel properties of CoCrFeNiMn high-entropy alloy fabricated by mechanical alloying and spark plasma sintering, Intermetallics 56 (2015) 24–27.
[32] S. Das, P.S. Robi, Mechanical alloying of W-Mo-V-Cr-Ta high entropy alloys.